

Turbulent natural convection along a vertical plate immersed in a stably stratified fluid

EVGENI FEDOROVICH† AND ALAN SHAPIRO

School of Meteorology, University of Oklahoma, 120 David L. Boren Blvd, Norman,
OK 73072-7307, USA

(Received 20 August 2007; revised 17 April 2009; accepted 17 April 2009)

The paper considers the moderately turbulent natural convection flow of a stably stratified fluid along an infinite vertical plate (wall). Attention is restricted to statistically stationary flow driven by constant surface forcing (heating), with Prandtl number of unity. The flow is controlled by the surface energy production rate F_s , molecular viscosity/diffusivity ν and ambient stratification in terms of the Brunt–Väisälä (buoyancy) frequency N . Following the transition from a laminar to a turbulent regime, the simulated flow enters a quasi-stationary oscillatory phase. In this phase, turbulent fluctuations gradually fade out with distance from the wall, while periodic laminar oscillations persist over much larger distances before they fade out. The scaled mean velocity, scaled mean buoyancy and scaled second-order turbulence statistics display a universal behaviour as functions of distance from the wall for given value of dimensionless combination $F_s/(\nu N^2)$ that may be interpreted as an integral Reynolds number. In the conducted numerical experiments, this number varied in the range from 2000 to 5000.

1. Introduction

Unsteady natural convection flows abound in nature and technology. Such flows are notoriously difficult to analyse theoretically because of the intrinsic coupling between the temperature and velocity fields. The case of unsteady laminar one-dimensional natural convection along an infinite vertical plate (sometimes referred to as a double-infinite plate because no leading or trailing edges are considered) provides one of the few scenarios where the Boussinesq equations of motion and thermodynamic energy may be solved analytically (Gebhart *et al.* 1988). Analytical solutions for unsteady one-dimensional natural convection along an infinite vertical plate were obtained in the 1950s and 1960s for a variety of surface forcings, though with a restriction to unstratified environments. The stability of these unstratified flows was analysed by Armfield & Patterson (1992) and Daniels & Patterson (1997, 2001). The extension of the one-dimensional convection framework to include ambient stratification is a relatively recent development (Park & Hyun 1998; Park 2001; Shapiro & Fedorovich 2004*a, b*, 2006).

Shapiro & Fedorovich (2004*b*) considered unsteady laminar natural convection in a stratified flow adjacent to a single infinite vertical plate (wall). Analytical solutions were obtained for a Prandtl number of unity for the cases of impulsive (step) change in plate perturbation temperature, sudden application of a plate heat flux and for

† Email address for correspondence: fedorovich@ou.edu

arbitrary temporal variations in plate perturbation temperature or plate heat flux. Vertical motion in a stably stratified fluid was associated with a simple negative feedback mechanism: rising warm fluid cooled relative to the environment, whereas subsiding cool fluid warmed relative to the environment. Because of this feedback, the laminar convective flow in stably stratified fluid adjacent to a double-infinite plate eventually approached a steady state, whereas the corresponding flow in an unstratified fluid did not.

In a companion paper, Shapiro & Fedorovich (2004a) explored the Prandtl number dependence of unsteady laminar natural convection of a stably stratified fluid along a single vertical plate both numerically and analytically. The developing boundary layers were thicker, more vigorous, and more sensitive to the Prandtl number at smaller Prandtl numbers (<1) than at larger Prandtl numbers (>1). The gross temporal behaviour of the flow after the onset of convection was of oscillatory-decay type for Prandtl numbers near unity, and of non-oscillatory-decay type for large Prandtl numbers. Stability analyses of the steady-state versions of these flows were conducted by Gill & Davey (1969) and Bergholz (1978).

In the context of turbulent natural convection, Phillips (1996) and Versteegh & Nieuwstadt (1998, 1999) numerically studied the flow of an unstratified fluid in a slot between two differentially heated vertical walls. In the direct numerical simulation (DNS) study of Versteegh & Nieuwstadt (1999), the extension of a two-region inner/outer scaling method of George & Capp (1979) for a turbulent convection flow along a single wall was employed to determine the basic functional dependencies (scaling laws) relating the mean and turbulent flow variables to the governing parameters and suitably normalized distance from the wall. Comparing the scalings proposed by George & Capp (1979) with the DNS results, Versteegh & Nieuwstadt (1999) concluded that the mean temperature profile and temperature variance were in a good agreement with the theoretical scalings, but the mean velocity profile and velocity variances were not. However, one should take into account that the Versteegh & Nieuwstadt (1999) study was concerned with one-dimensional flow between two double-infinite walls, while George & Capp (1979) considered the two-dimensional flow along a single semi-infinite wall (in the presence of leading edge). A finding of particular importance, based on the DNS results of Versteegh & Nieuwstadt (1999) and on the laboratory data of Boudjemadi *et al.* (1997), was that of the exchange coefficient becoming negative in a layer near the wall. This implies that the commonly adopted gradient transfer hypothesis breaks down in the near-wall region of the studied convection flow, in contrast to the situation in conventional wall-bounded flows (Tennekes & Lumley 1972).

It should be born in mind, however, that these preceding studies have all been conducted with unstratified fluids. As it is well known from geophysical fluid dynamics, stratification plays a crucial role in the structure of turbulent flows (Cushman-Roisin 1994). Moreover, in the specific context of semi-infinite vertical-plate (wall) convection, the fully developed boundary layer flow is height-dependent over the entire wall in the case of unstratified fluid, while the fully developed flow in stratified fluid is height-dependent only in the region of the leading edge (Armfield, Patterson & Lin 2007), with the flow solution becoming height-independent at large distances along the wall.

To our knowledge, the structure of turbulent natural convection flow along a vertical heated wall in the presence of ambient stratification has not been studied by means of DNS so far. The present paper considers the same physical scenario as in Shapiro & Fedorovich (2004b), that is, natural convection along an infinite vertical wall in a stably stratified fluid, but for the surface buoyancy forcing large enough

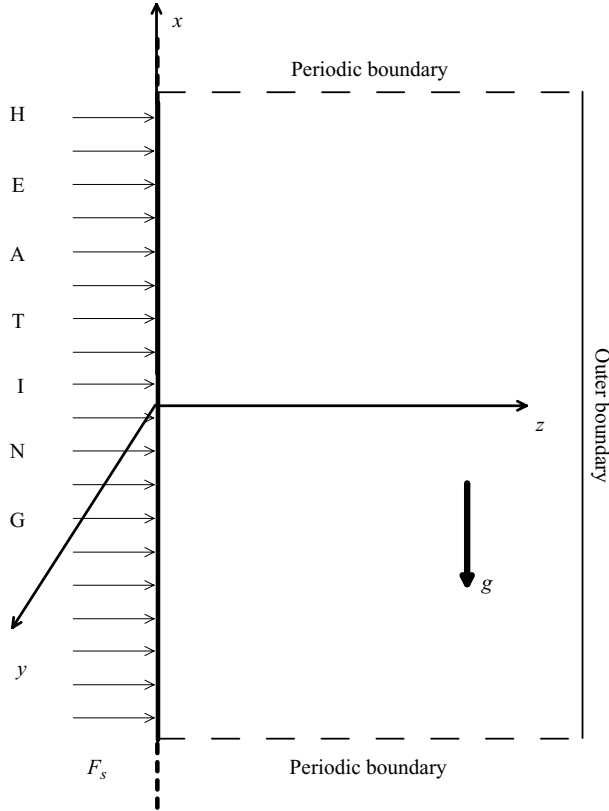


FIGURE 1. Schematic of the flow along a heated wall.

that the flow becomes turbulent. Attention is restricted to the case of convection flow driven by constant surface buoyancy flux, with Prandtl number of unity. DNS is employed as the basic tool of the study, and the numerical results are analysed at times large enough that a statistically stationary state has been achieved.

2. Governing equations

The three-dimensional Boussinesq equations of motion, thermodynamic energy and mass conservation in a right-hand Cartesian (x, y, z) coordinate system attached to the wall are (Shapiro & Fedorovich 2004a):

$$\frac{\partial u_i}{\partial t} + u_j \frac{\partial u_i}{\partial x_j} = -\frac{\partial p''}{\partial x_i} + \beta T'' \delta_{i1} + \nu \frac{\partial^2 u_i}{\partial x_j \partial x_j}, \quad (1)$$

$$\frac{\partial T''}{\partial t} + u_j \frac{\partial T''}{\partial x_j} = -\gamma u_1 + \kappa \frac{\partial^2 T''}{\partial x_j \partial x_j}, \quad (2)$$

$$\frac{\partial u_i}{\partial x_i} = 0, \quad (3)$$

where $i = 1, 2, 3$, $j = 1, 2, 3$, $\mathbf{u} = (u_1, u_2, u_3) \equiv (u, v, w)$ is the three-dimensional velocity vector with the components along the coordinate axes $x \equiv x_1$ and $y \equiv x_2$ (the along-wall coordinates with x being vertical) and $z \equiv x_3$ (normal to the wall directed away from it) (see figure 1), $p'' = [p - p_\infty(x)]/\rho_r$ is the normalized deviation of pressure p

from its hydrostatic value $p_\infty(x)$ far away from the wall, ρ_r is a constant reference density, $T'' = T - T_\infty(x)$ is the perturbation temperature, $T_\infty(x)$ is a linearly varying ambient temperature far away from the wall, $\gamma \equiv dT_\infty/dx + g/c_p$ is the stratification parameter, ν is the kinematic viscosity, κ is the molecular thermal diffusivity, $\beta = g/T_r$ is the buoyancy parameter (g is the gravitational acceleration and T_r is a constant reference temperature), δ_{ij} is the Kronecker delta and the Einstein rule of summation over repeated indices is applied.

In terms of buoyancy $b \equiv -g \frac{\rho - \rho_\infty(x)}{\rho_r} \simeq g \frac{T - T_\infty(x)}{T_r} = \beta T''$ (with ρ_∞ denoting the ambient density) and Brunt–Väisälä (or buoyancy) frequency in the ambient stably stratified fluid $N = \sqrt{\gamma\beta}$, the governing equations (1)–(3) may be rewritten as

$$\frac{\partial u_i}{\partial t} + u_j \frac{\partial u_i}{\partial x_j} = -\frac{\partial p''}{\partial x_i} + b\delta_{i1} + \nu \frac{\partial^2 u_i}{\partial x_j \partial x_j}, \quad (4)$$

$$\frac{\partial b}{\partial t} + u_j \frac{\partial b}{\partial x_j} = -N^2 u_1 + \kappa \frac{\partial^2 b}{\partial x_j \partial x_j}, \quad (5)$$

$$\frac{\partial u_i}{\partial x_i} = 0. \quad (6)$$

These equations are to be applied to a fluid bounded by a single double-infinite vertical wall (no leading edge) in an otherwise unbounded domain. The wall is located at $z=0$. The surface forcing (buoyancy flux specified at the wall surface) is temporally constant and uniform along the wall.

We apply in (4)–(6) the Reynolds decomposition of flow fields (Pope 2000): $\varphi = \bar{\varphi}(z) + \varphi'(t, x, y, z)$, where φ is a generic flow variable, $\bar{\varphi}(z)$ is its average value that depends only on the distance from the wall and $\varphi'(t, x, y, z)$ is the turbulent perturbation of φ . Averaging (4)–(6) spatially (over x – y planes) and temporally (over t), and applying the surface conditions of impermeability ($w=0$ at $z=0$) and no slip ($u=v=0$ at $z=0$), we reduce the system (4)–(6) to

$$b + \nu \frac{\partial^2 \bar{u}}{\partial z^2} - \frac{\partial \overline{u'w'}}{\partial z} = 0, \quad (7)$$

$$-uN^2 + \kappa \frac{\partial^2 \bar{b}}{\partial z^2} - \frac{\partial \overline{b'w'}}{\partial z} = 0, \quad (8)$$

$$-\frac{\partial \overline{p''}}{\partial z} - \frac{\partial \overline{w'w'}}{\partial z} = 0, \quad (9)$$

where (9) immediately integrates to the relationship $\overline{p''} = -\overline{w'w'}$ (where we have assumed that $\overline{w'w'}$ vanishes at $z=\infty$). In (7) and (8), \bar{b} now denotes mean buoyancy and \bar{u} denotes the mean flow velocity component along the wall (with overbars omitted), while $\overline{u'w'}$ and $\overline{b'w'}$ represent z components of turbulent kinematic fluxes of mean momentum and buoyancy, respectively. In the remainder of this study, we will restrict our attention to a Prandtl number of unity ($Pr = \nu/\kappa = 1$).

At the surface (denoted by the subscript s), the flow should satisfy the no-slip condition, so $u_s \equiv u(0) = 0$, and a constant surface buoyancy flux $-\nu(\partial b/\partial z)|_s = F_s$ is prescribed. For the case of a heated wall, $F_s > 0$. At very large distances from the wall, the flow disturbance induced by the heated wall is expected to vanish, so $u=0$ and $b=0$ as $z \rightarrow \infty$. From no-slip and impermeability conditions, it follows that turbulent fluxes $\overline{u'w'}$ and $\overline{b'w'}$ must both vanish at $z=0$. Furthermore, we assume that these fluxes vanish as $z \rightarrow \infty$. With such boundary conditions, the surface energy production rate F_s , kinematic diffusivity ν and ambient stratification frequency N

completely determine the structure of the considered turbulent natural convection flow.

3. Numerical simulation

3.1. Numerical algorithm

The considered flow case is investigated by means of DNS. The DNS algorithm employed to solve (4)–(6) with $Pr = \nu/\kappa = 1$ is generally the same as that used to reproduce laminar convection regimes in Shapiro & Fedorovich (2004a) and previously applied for the large eddy simulation of laboratory and atmospheric convective boundary layers in Fedorovich, Nieuwstadt & Kaiser (2001); Fedorovich *et al.* (2004a); Fedorovich, Conzemius & Mironov (2004b). In the current version of the numerical code, the time advancement is performed by a hybrid leapfrog/Adams–Moulton third-order scheme (Shchepetkin & McWilliams 1998). The spatial derivatives are approximated by second-order finite-difference expressions on a staggered grid. The Poisson equation for pressure is solved with a fast Fourier transform technique over the x – y planes and a tri-diagonal matrix inversion method in the wall-normal direction. No-slip and impermeability conditions are applied on the velocity field at the wall. The third equation of motion is used as a boundary condition for the pressure at the wall and at the outer boundary of the domain (large z). Normal gradients of prognostic variables (velocity components and buoyancy) are set to zero at the outer boundary of the computational domain, and periodic boundary conditions are imposed at the x – z and y – z boundaries of the domain.

In the simulations, we tried to reproduce a representative variety of turbulent flow regimes without going beyond the capabilities of the numerical scheme employed or straining computer resources (all simulations have been performed on a standard two-processor workstation). For these two reasons, we limited the maximum Reynolds number (Re) value to 5000 (the method used for evaluating Re in our experiments will be explained in §4). This value was large enough to obtain reasonably developed turbulence while allowing use of relatively compact numerical grids and providing sufficiently long time series of variables to track the flow development. The simulations described in this paper were conducted on the $(x \times y \times z) = 256 \times 256 \times N_z$ uniformly spaced ($\Delta x = \Delta y = \Delta z = \Delta$) grids, with N_z depending on the Re number of the simulated flow ($N_z = 600$ in the flow case with $Re = 5000$). The grid spacing Δ was chosen to ensure that the resolvability condition $\Delta \lesssim (\pi/1.5)L_m$ is satisfied (Pope 2000), where $L_m = \min(\nu^{3/4}F_s^{-1/4}, F_s^{1/2}N^{-3/2})$ with $\nu^{3/4}F_s^{-1/4}$ and $F_s^{1/2}N^{-3/2}$ being, respectively, analogues of the Kolmogorov microscale (Tennekes & Lumley 1972) and of the Ozmidov length scale commonly encountered in oceanography (Smyth & Moum 2000). Numerical experiments in which the grid spacing and size were varied individually by factors between 0.5 and 2 showed that, once the resolvability condition was satisfied, the dependence of the mean flow and turbulence statistics on the grid cell size and domain dimensions was very minor, with the discrepancies being of the order of a per cent and less.

3.2. Convection flow structure

Figure 2 shows the spatial (in the z direction) and temporal evolution of the velocity (u component) and buoyancy fields in the central point of the x – y plane from the simulation with $F_s = 0.5 \text{ m}^2 \text{ s}^{-3}$, $\nu = 10^{-4} \text{ m}^2 \text{ s}^{-1}$, $N = 1 \text{ rad s}^{-1}$ and $\Delta = 0.0025 \text{ m}$. After the transition stage that takes about one period of gravity-wave oscillation ($2\pi/N$), both fields reveal the essentially turbulent nature of the flow close to the

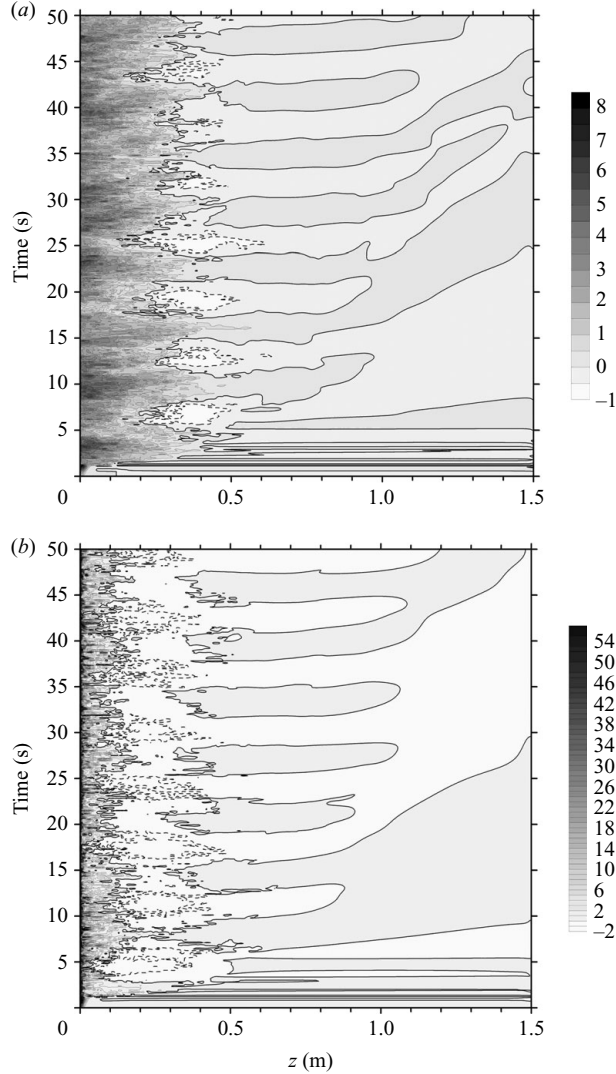


FIGURE 2. Spatial and temporal evolution of (a) velocity (in m s^{-1}) and (b) buoyancy (in m s^{-2}) fields in the central point of the x - y plane for the flow case with $F_s = 0.5 \text{ m}^2 \text{ s}^{-3}$, $\nu = 10^{-4} \text{ m}^2 \text{ s}^{-1}$ and $N = 1 \text{ rad s}^{-1}$. Negative contours are dashed. Zero contours are marked by bold solid lines.

heated wall and an oscillatory quasi-periodic behaviour of the flow at larger distances from the wall. In the immediate vicinity of the wall, the flow remains quasi-laminar. With increasing distance from the wall, turbulent fluctuations develop on a relatively broad scale range. However, only fluctuations with a frequency equal to the natural buoyancy frequency N dominate at larger distances from the wall. Fluctuations with other frequencies decay more rapidly away from the wall. These dominant oscillations are apparent far beyond the thermal and dynamic turbulent boundary layers (see figure 3).

A similar oscillatory flow pattern at large distances from the wall was observed in the Shapiro & Fedorovich (2006) study of a laminar natural convection flow along a

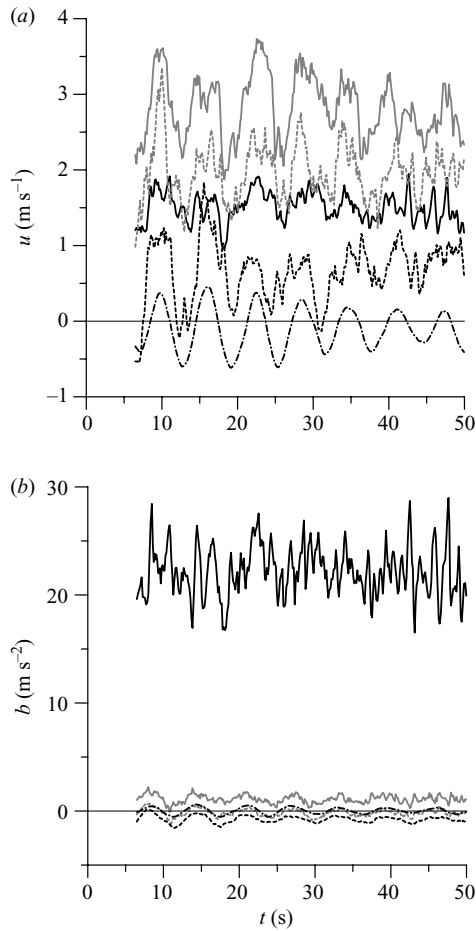


FIGURE 3. Time series of mean velocity (a) and buoyancy (b) for the same flow case as in figure 2 at different distances from the wall: 0.00125 m (solid black line), 0.0625 m (solid grey line), 0.125 m (dashed grey line), 0.25 m (dashed black line) and 0.5 m (dashed and dotted black line) from the wall.

wall with a temporally periodic surface thermal forcing. In the present case, however, the oscillatory flow motions result from interactions between turbulence and ambient stable stratification under the conditions of a temporally constant surface buoyancy forcing.

Flow fields in figures 2 and 3 also reveal that the boundary-layer flow along the wall becomes statistically stationary as time grows. Remarkably, the thermal boundary layer, whose depth may be estimated from the position of a convoluted contour of zero buoyancy in figure 2(b), is much shallower than the dynamic (momentum) boundary layer in figure 2(a). Figure 3 displays time series of simulated velocity and buoyancy fields at different distances from the wall for the same flow case. The relative shallowness of the thermal boundary layer, noted above, is manifested in figure 3(b) by the fast drop of buoyancy away from the wall. Another previously discussed feature of the flow, the persistent oscillatory fluctuations of the flow fields with frequency N at large distances from the wall, is also clearly seen in figure 3.

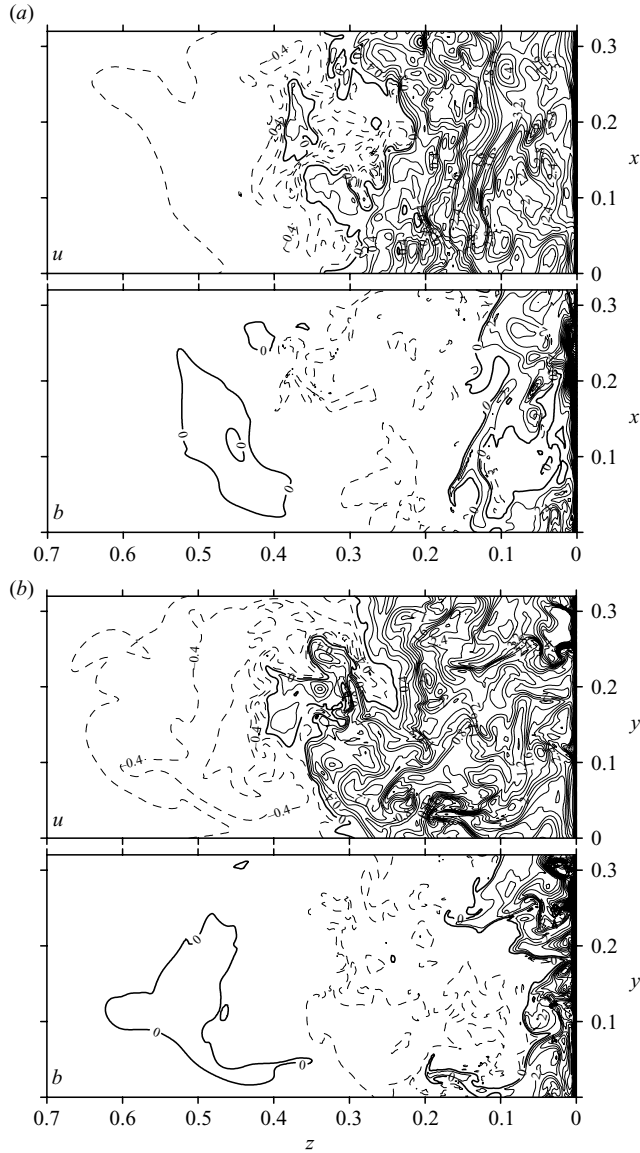


FIGURE 4. (a) Buoyancy (b , in m s^{-2}) and (b) velocity (u , in m s^{-1}) fields over $x-z$ (a) $y-z$ (b) cross-sections of the numerical domain at $t = 49.1$ s (which corresponds to about eight oscillation periods) for the flow case shown in figures 2 and 3. Distances are indicated in metres. Negative contours are dashed. Zero contours are marked by bold solid lines.

Insight into the spatial structure of the turbulent convection flow at a fixed time in the simulation may be gained from the snapshots of the flow cross-sections shown in figure 4. Both buoyancy and velocity fields exhibit a markedly irregular behaviour typical of a developed turbulent flow. The buoyancy fluctuations reach their maximum magnitude in the close vicinity of the wall, while the velocity fluctuations appear to be largest at distances from the wall roughly corresponding to the position of the convoluted interface separating regions of positive and negative buoyancy. Buoyancy

fluctuations in the relatively deep region of negative buoyancy are rather weak and lack any remarkable structural features.

On the other hand, the structure of the velocity field in the area of maximum intensity of velocity fluctuations at z about 0.15 m in the $x-z$ cross-section shows a moderate degree of coherence, with velocity fluctuations being organized in elongated streaks directed along the mean flow. In the $y-z$ cross-section, the projections of these streaks appear as organized structures oriented along z . At larger distances from the wall, this feature disappears, and velocity fluctuations in both the $x-z$ and $y-z$ planes become more isotropic. In the flow region around $z=0.3$ m, zones of positive and negative velocity fluctuations coexist, and one can see splashes of positive momentum penetrating rather deeply into the region with overall negative velocity values.

This reverse flow, along with the offset negative buoyancy region, is a signature feature of the simulated convection flow in the presence of stable stratification. In the case of an unstratified flow simulation with $N=0$ (not shown), the reverse flow and the negative buoyancy patch do not develop, and regions of positive momentum and buoyancy persistently grow in depth with time.

3.3. Mean profiles and turbulence statistics

Figure 5 shows the mean flow profiles and kinematic fluxes of momentum and buoyancy for four flow cases with $\nu=10^{-4}$ m²s⁻¹ and $N=1$ s⁻¹, surface buoyancy flux F_s ranging from 0.2 to 0.5 m²s⁻³, and grid spacing $\Delta=0.0025$ m. These profiles were obtained by averaging the flow fields spatially over $x-y$ planes and temporally over seven oscillation periods beyond the transition stage. The dimensional profiles of mean buoyancy and along-wall velocity show considerable sensitivity to F_s . For instance, the velocity maximum in the case of $F_s=0.5$ m²s⁻³ is almost twice as large as in the case of $F_s=0.2$ m²s⁻³. The differences between buoyancy profiles corresponding to different F_s are largest in the close vicinity of the wall. The difference in depth between the thermal and dynamic boundary layers, already noted above, is clearly seen from comparing the rate of decay of buoyancy with distance from the wall to that of velocity after it reached its maximum in close vicinity of the wall. Velocity gradients on the left of the maximum, in the inner flow region, are markedly larger than those on the outer side. This pronounced asymmetry of the velocity maximum increases with growing F_s . The region of reverse mean flow (negative u) in figure 5(a) is narrower than the zone of negative mean buoyancy and is shifted outwards (larger z) with respect to the buoyancy minimum. The overall depths of both the reverse flow and region of negative buoyancy grow with F_s . Although there are large quantitative differences between the turbulent flow and the corresponding laminar flow (Shapiro & Fedorovich 2004b), the basic mean flow structure is qualitatively the same: warm (relative to environment) fluid rises along the wall, whilst cool fluid subsides at some distance from the wall.

Large relative differences between second-order turbulence statistics (kinematic fluxes and variances) for flows with different surface forcing intensities are apparent in figures 5(b) and 6. Greater F_s values lead to larger magnitudes of both fluxes and variances. As seen in figure 5, zero crossings in the mean profiles of b and u are quite precisely co-located with the minima and maxima of the fluxes $\overline{u'w'}$ and $\overline{b'w'}$, as predicted by (7) and (8). It can also be seen in figure 5 that positions of zero fluxes are closely associated with positions of zero gradients of corresponding mean profiles. Moreover, throughout the whole flow, there is an apparent anti-correlation between the turbulent fluxes and the gradients. These features allow us to infer that close flux-gradient relationships in terms of positive exchange coefficient are valid

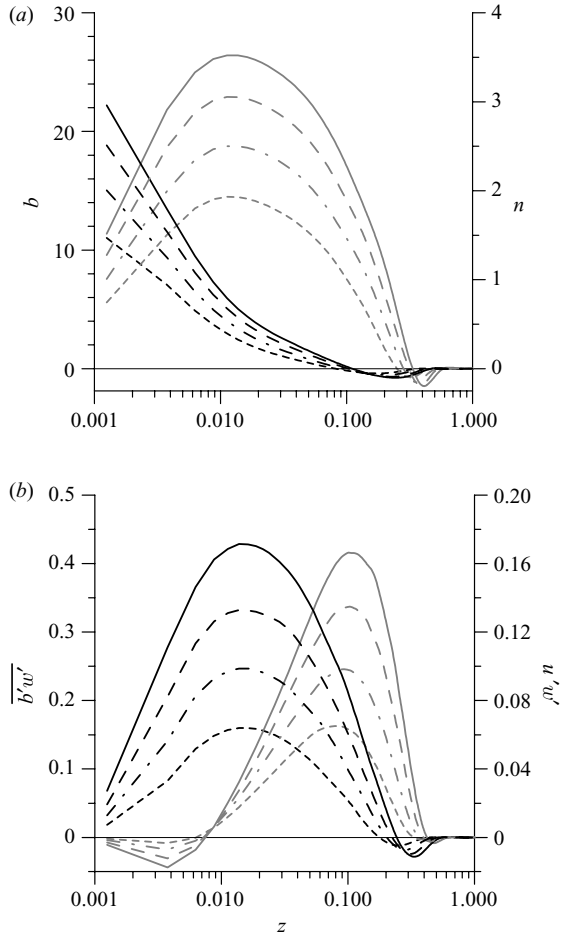


FIGURE 5. Profiles of (a) mean flow buoyancy (in m s^{-2} ; black) and velocity (in m s^{-1} ; grey), and (b) of kinematic fluxes of buoyancy (in $\text{m}^2 \text{s}^{-3}$; black) and momentum (in $\text{m}^2 \text{s}^{-2}$; grey) for the flow cases with $\nu = 10^{-4} \text{ m}^2 \text{ s}^{-1}$, $N = 1 \text{ rad s}^{-1}$ and F_s equal to 0.2 (short-dash lines), 0.3 (dashed and dotted lines), 0.4 (long-dash lines) and 0.5 (solid lines) $\text{m}^2 \text{ s}^{-3}$. Distances are indicated in metres.

throughout the entire simulated flow, even in the very close vicinity of the wall, in contrast to the near-wall region of the unstratified flow in a double-wall channel simulation of Versteegh & Nieuwstadt (1999).

Figure 5 also shows that positive peaks of both $\overline{u'w'}$ and $\overline{b'w'}$ fluxes are rather narrow (especially, that of the buoyancy flux), and there is no indication of any extended flow region with constancy (even approximate) of any flux with distance from the wall. In more conventional boundary-layer type flows, driven, for instance, by imposed pressure gradient along the wall, the existence of distance intervals with constant (slowly varying) momentum and buoyancy fluxes is used as a foundation for similarity analyses and scalings. Clearly, such a constant-flux formalism would not apply, at least in a straightforward manner, to the flow that is considered in our study. Furthermore, we did not find any evidence of scale separation in the simulated flow cases that would allow the flow to be subdivided into regions where any of the three governing parameters (F_s , ν , N) could be dropped from consideration. For instance,

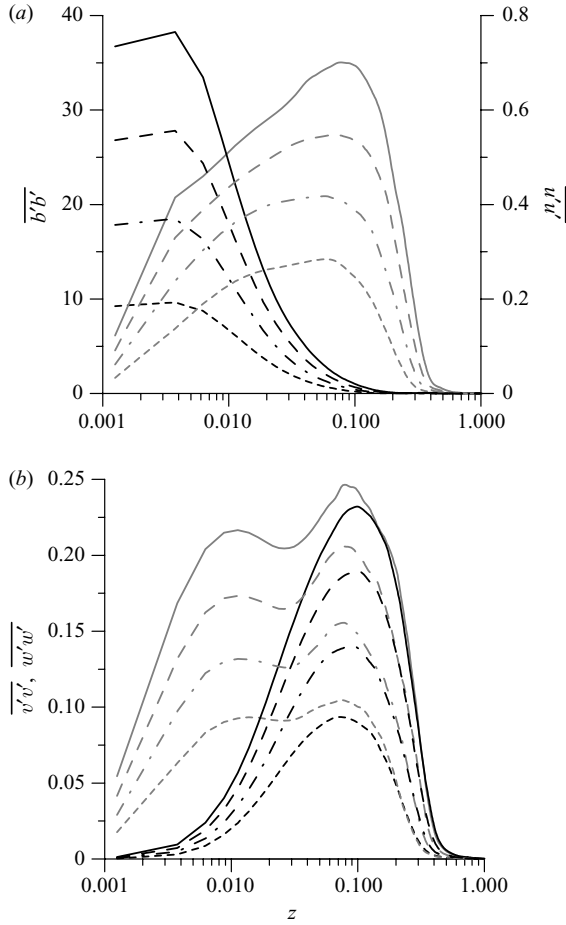


FIGURE 6. Profiles of variances of (a) buoyancy (in $\text{m}^2 \text{s}^{-4}$; black) and u velocity component (in $\text{m}^2 \text{s}^{-2}$; grey), and (b) w (in $\text{m}^2 \text{s}^{-2}$; black) and v (in $\text{m}^2 \text{s}^{-2}$; grey) velocity components for the flow cases with $\nu = 10^{-4} \text{m}^2 \text{s}^{-1}$, $N = 1 \text{rad s}^{-1}$ and F_s equal to 0.2 (short-dash lines), 0.3 (dashed and dotted lines), 0.4 (long-dash lines) and 0.5 (solid lines) $\text{m}^2 \text{s}^{-3}$. Distances are indicated in metres.

even at relatively large distances from the wall, the molecular viscosity/diffusivity in combination with surface buoyancy flux would influence the local flow structure through the near-wall peak velocity value that is directly determined by their combined effect. Analogously, the influence of stratification (in terms of N) is started to be felt in the simulated flow already in the immediate vicinity of the wall, so it would be impossible to isolate a flow region where dependence on N may be neglected. The above conclusions based on the observations of the simulated flow structure are supported by scaling considerations presented in §4.

As profiles of the buoyancy variance in figure 6(a) reveal, the buoyancy fluctuations attain their maximum magnitude extremely close to the wall (again note logarithmic scaling of z in the plot), even closer to the wall than the location of the peak mean velocity. The drop of $\overline{b'b'}$ beyond the maximum is also rather fast; significant fluctuations of the buoyancy are restricted to a comparatively thin near-wall layer. Velocity fluctuations, on the other hand, grow in magnitude relatively slowly with

distance from the wall, with $\overline{u'u'}$ reaching its maximum at a location, where the buoyancy variance has dropped to very low levels. The post-maximum decay of $\overline{u'u'}$ is also much more gradual than that of $\overline{b'b'}$. Overall, the velocity fluctuations of notable magnitudes are distributed over a layer that is a few times thicker than the layer which contains buoyancy fluctuations. Development of velocity fluctuations normal to the wall is apparently hampered by the presence of the wall. This explains the relatively slow growth of $\overline{w'w'}$ with z (figure 6*b*) compared to $\overline{u'u'}$ in figure 6(*a*) and $\overline{v'v'}$ in figure (6*b*). Curiously, profiles of the latter variance for different F_s consistently display secondary maxima very close to the wall, at distances comparable to those at which mean velocity maxima occur (see figure 6*a*). To explain these secondary maxima in $\overline{v'v'}$, the estimates of second-order turbulence moment budgets would be needed, but those are not available at this point. Profiles of crossflow (v and w) velocity variances for given F_s overlap beyond their maxima and, at larger distances from the wall ($z > 0.3$ m), follow rather closely the profiles of $\overline{u'u'}$. This behaviour of the variances points to an isotropization of the velocity fluctuations with increasing distance from the wall. This is another feature that could be investigated by means of evaluating budgets of variances of the individual velocity components.

4. Scaling considerations

Noting that in the case of $Pr = 1$ ($\nu = \kappa$) the governing parameters of the flow ν , N and F_s have, respectively, dimensions of $[L^2 T^{-1}]$, $[T^{-1}]$ and $[L^2 T^{-3}]$, and introducing generic scales L (for distance), V (for velocity), and B (for buoyancy), the Π theorem (Langhaar 1951) allows us to write

$$L = \nu^{1/2} N^{-1/2} f_L(F_s \nu^{-1} N^{-2}), \quad V = \nu^{1/2} N^{1/2} f_V(F_s \nu^{-1} N^{-2}),$$

$$B = \nu^{1/2} N^{3/2} f_B(F_s \nu^{-1} N^{-2}), \quad (10)$$

where f_L , f_V and f_B are dimensionless functions of the dimensionless combination (number) $F_s \nu^{-1} N^{-2}$. This combination may be interpreted as an integral Reynolds number of the flow. Indeed, integrating (8) over z from 0 [where $\overline{b'w'} = 0$ and $\kappa(\partial b/\partial z) = \nu(\partial b/\partial z) = -F_s$] to ∞ (where $\overline{b'w'} = 0$ and $\partial b/\partial z = 0$), we come to

$$\frac{\tilde{V}\tilde{L}}{\nu} \equiv \frac{\int_0^\infty u \, dz}{\nu} = \frac{F_s}{\nu N^2} \equiv Re, \quad (11)$$

where $\tilde{L} \equiv \frac{1}{V} \int_0^\infty u \, dz$ and \tilde{V} are integral length and velocity scales of the considered flow.

Expression (11) also provides an integral constraint for the velocity profile: $\int_0^\infty u \, dz = F_s/N^2$, which indicates that the velocity integral does not depend on the viscosity/diffusivity and is entirely determined by the ratio of the surface buoyancy forcing to the ambient stratification strength in terms of N^2 . By calculating integrals of the simulated velocity profiles shown in figure 5(*a*), we evaluated this constraint and found it to be valid within a single per cent accuracy.

The Shapiro & Fedorovich (2004*b*) length, velocity and buoyancy scales for the laminar convection (they may be called the laminar or l -scales),

$$L = \nu^{1/2} N^{-1/2} \equiv L_l, \quad V = F_s \nu^{-1/2} N^{-3/2} \equiv V_l, \quad B = F_s \nu^{-1/2} N^{-1/2} \equiv B_l, \quad (12)$$

are particular cases of the scales (10) that correspond to $f_L = 1$, $f_V = Re$ and $f_B = Re$. This scaling provides the following l -scaled equations of mean momentum and buoyancy balance:

$$b_l + \frac{\partial^2 u_l}{\partial z_l^2} - Re \frac{\partial \tau_l}{\partial z_l} = 0, \quad (13)$$

$$-u_l + \frac{\partial^2 b_l}{\partial z_l^2} - Re \frac{\partial F_l}{\partial z_l} = 0, \quad (14)$$

$$u_l = 0 \text{ and } \partial b_l / \partial z_l = -1 \text{ at } z_l = 0, \quad (15)$$

$$u_l = 0 \text{ and } b_l = 0 \text{ as } z_l \rightarrow \infty, \quad (16)$$

where $Re = V_l L_l / \nu = F_s \nu^{-1} N^{-2}$, $z_l = z / L_l$, $u_l = u / V_l$, $b_l = b / B_l$, $\tau_l = (\overline{u'w'})_l = \overline{u'w'} / V_l^2$, and $F_l = (\overline{b'w'})_l = \overline{b'w'} / (V_l B_l)$. Dimensionless quantities u_l , b_l , τ_l and F_l in (13)–(16) should universally depend on z_l for all ν , N and F_s that produce, in combination, the same value of $Re = F_s \nu^{-1} N^{-2}$.

The deduced universal behaviour of the scaled flow fields provides a framework for testing the appropriateness of the numerical procedure applied to simulate the flow. Indeed, by keeping the grid spacing and the domain size constant, and varying values of ν , N and F_s , we implicitly prescribe different ratios between Δ and L_m [under the constraint $\Delta \lesssim (\pi/1.5)L_m$ (see §3.1)], as well as between Δ and the domain size. By varying the basic parameters of the flow in this manner, we also test the statistical adequacy of the calculated turbulence moments.

First, we demonstrate that our numerical code is able to reproduce the universality of the mean velocity and buoyancy profiles for the flow cases with two different Re numbers (3000 and 4000).

The first considered flow case with $Re = 3000$ is one of the flow cases (with $F_s = 0.3 \text{ m}^2 \text{ s}^{-3}$, $\nu = 10^{-4} \text{ m}^2 \text{ s}^{-1}$, and $N = 1 \text{ s}^{-1}$) previously examined in §3. For this flow case: $\Delta = 0.0025 \text{ m}$ and $L_m = \nu^{3/4} F_s^{-1/4} = 0.00135 \text{ m}$ (see §3.1). The second simulated case with $Re = 3000$ and $\Delta = 0.0025 \text{ m}$ differs from the first one by setting values of the governing parameters to $F_s = 0.9 \text{ m}^2 \text{ s}^{-3}$, $\nu = \sqrt{3} \times 10^{-4} \text{ m}^2 \text{ s}^{-1}$ and $N = \sqrt[4]{3} \text{ rad s}^{-1}$ (this provides $L_m = 0.00155 \text{ m}$).

In the case of $Re = 4000$, the simulated flow with $\Delta = 0.0025 \text{ m}$, $F_s = 0.4 \text{ m}^2 \text{ s}^{-3}$, $\nu = 10^{-4} \text{ m}^2 \text{ s}^{-1}$ and $N = 1 \text{ s}^{-1}$ (corresponding to $L_m = 0.00126 \text{ m}$), also considered in §3, is compared to the flow with $\Delta = 0.0025 \text{ m}$, $F_s = 0.8 \text{ m}^2 \text{ s}^{-3}$, $\nu = \sqrt{2} \times 10^{-4} \text{ m}^2 \text{ s}^{-1}$ and $N = \sqrt[4]{2} \text{ rad s}^{-1}$ (corresponding to $L_m = 0.00137 \text{ m}$).

For all these cases, the velocity and buoyancy fields from the DNS output were averaged over time and x – y planes in the manner described in §3 and then scaled with corresponding l -scales of velocity and buoyancy before being plotted against non-dimensional z_l . The scaled profiles of velocity and buoyancy shown in figures 7(b) and 7(d) clearly confirm that computed normalized u and b indeed perform in a universal manner with different sets of ν , N and F_s that combine into the same $Re = F_s \nu^{-1} N^{-2}$.

The universal behaviour is also observed in the scaled profiles of the $Re = 3000$ case kinematic fluxes of buoyancy $\overline{b'w'}$ and momentum $\overline{u'w'}$, represented in the scaled equations (13) and (14), as well as in the buoyancy $\overline{b'b'}$ and velocity $\overline{u'u'}$ variances (see figure 8). These simulation results demonstrate the overall similarity of turbulence structure in convection flows of same Re and also suggest that computational parameters and averaging procedures adopted for the simulations and have been chosen adequately.

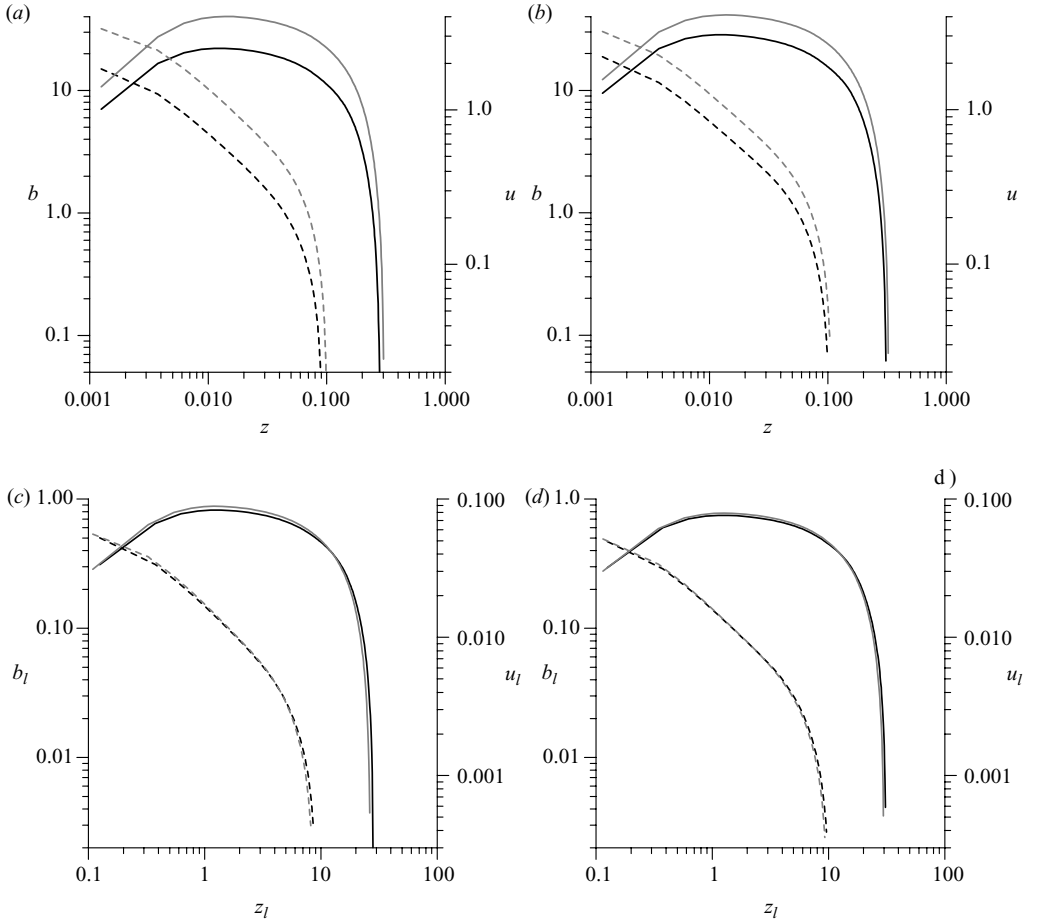


FIGURE 7. Original ((a) and (b) with buoyancy in m s^{-2} , velocity in m s^{-1} , distances in metres) and l -scaled (c and d) profiles of mean buoyancy (dashed lines) and velocity (solid lines) for flow cases with $Re = 3000$ (a and c) and $Re = 4000$ (b and d). In (a) and (c), black lines refer to the case of $\nu = 10^{-4} \text{ m}^2 \text{ s}^{-1}$, $N = 1 \text{ rad s}^{-1}$, $F_s = 0.3 \text{ m}^2 \text{ s}^{-3}$ and grey lines refer to the case of $\nu = \sqrt{3} \times 10^{-4} \text{ m}^2 \text{ s}^{-1}$, $N = \sqrt[4]{3} \text{ rad s}^{-1}$, $F_s = 0.9 \text{ m}^2 \text{ s}^{-3}$. In (b) and (d), black lines refer to the case of $\nu = 10^{-4} \text{ m}^2 \text{ s}^{-1}$, $N = 1 \text{ rad s}^{-1}$, $F_s = 0.4 \text{ m}^2 \text{ s}^{-3}$ and grey lines refer to the case of $\nu = \sqrt{2} \times 10^{-4} \text{ m}^2 \text{ s}^{-1}$, $N = \sqrt[4]{2} \text{ rad s}^{-1}$, $F_s = 0.8 \text{ m}^2 \text{ s}^{-3}$.

5. Conclusions

Turbulent natural convection flow along a double-infinite heated vertical plate (wall) immersed in a stably stratified fluid has been investigated numerically by means of DNS. The considered flow is driven by a maintained spatially uniform wall buoyancy flux. To our knowledge, this is the first DNS study of the structure of turbulent natural convection flow along a vertical heated wall in the presence of ambient stratification.

Following the transition from a laminar to a turbulent regime, the simulated flow enters a quasi-stationary oscillatory phase. In this phase, turbulent fluctuations gradually fade out with distance from the wall, while periodic laminar oscillations persist over much larger distances before they fade out. Such oscillatory flow motions result from interactions between turbulence and ambient stable stratification. It should

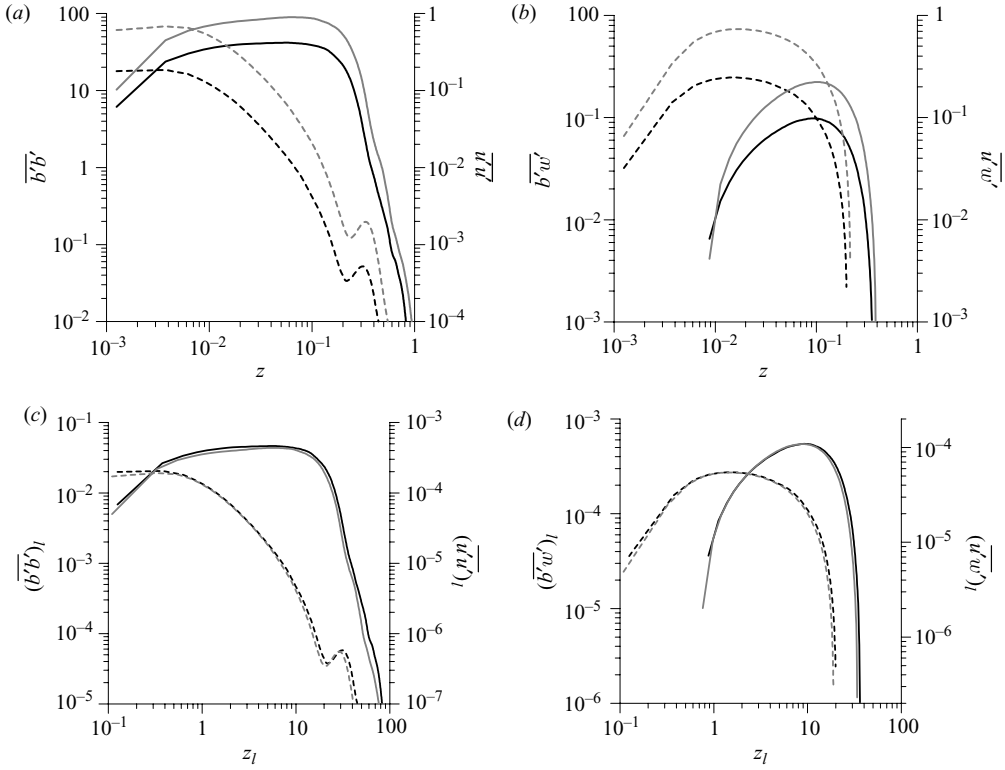


FIGURE 8. Original (*a* and *b*) and *l*-scaled (*c* and *d*) profiles of turbulent momentum (solid lines) and buoyancy (dashed lines) kinematic fluxes for flow cases with $Re = 3000$. Black lines refer to the case of $\nu = 10^{-4} \text{ m}^2 \text{ s}^{-1}$, $N = 1 \text{ rad s}^{-1}$, $F_s = 0.3 \text{ m}^2 \text{ s}^{-3}$ and grey lines refer to the case of $\nu = \sqrt{3} \times 10^{-4} \text{ m}^2 \text{ s}^{-1}$, $N = \sqrt[4]{3} \text{ rad s}^{-1}$, $F_s = 0.9 \text{ m}^2 \text{ s}^{-3}$. In (*a*) and (*b*), buoyancy is in m s^{-2} , buoyancy flux is in $\text{m}^2 \text{ s}^{-3}$, velocity variance and momentum flux are in $\text{m}^2 \text{ s}^{-2}$ and distances are in metres.

be stressed that this oscillatory flow occurs under the conditions of a temporally constant surface buoyancy forcing.

The basic structure of the mean flow (averaged over time and wall-parallel planes) is similar to that of the laminar convection: warm (relative to environment) fluid rises along the wall, whilst cool fluid subsides at some distance from the wall. Close relations between the gradients of mean fields and intensities of corresponding turbulent fluxes are observed over the simulated turbulent flow. This implies that the turbulent fluxes are directed in a conventional manner that is opposite to the gradients of the corresponding mean fields, throughout the entire domain.

No extended flow region has been identified with constancy (even approximate) of any of the fluxes with distance from the wall. Consequently, a constant-flux formalism appears to be inapplicable to the simulated flow within the investigated parameter ranges. Moreover, no evidence has been found of scale separation in the simulated flow cases that would allow the flow to be subdivided into regions where any of governing parameters (F_s , ν , N) could be dropped from consideration.

The flow structure was found to be determined by a single dimensionless combination of the governing flow parameters $F_s \nu^{-1} N^{-2}$, which was shown to have a meaning of an integral Reynolds number. It was demonstrated that any

expressions for length L , velocity V and buoyancy B scales in terms of the governing parameters, should yield normalized profiles of velocity, buoyancy, and kinematic fluxes of momentum and heat that are universal functions of scaled distance from the wall for any particular $Re = F_s \nu^{-1} N^{-2}$. An integral constraint for the velocity profile, $\int_0^\infty u dz = F_s / N^2$, derived from the analysis of the governing flow equations, was confirmed by the numerical data.

Profiles of the crossflow velocity variance for different magnitudes of the surface forcing consistently display secondary maxima very close to the wall, at distances comparable to those of the mean velocity maxima. An explanation of this and other peculiar turbulence structure features, like the observed isotropization of the velocity fluctuations with increasing distance from the wall, would require estimates of the second-order turbulence moment budgets in the simulated flow and analyses of its turbulence spectra.

The first author acknowledges support from the National Center for Atmospheric Research (NCAR), USA, and inspiring discussions with Peter Sullivan during the intermediate stage of work on this paper. Valuable comments of four anonymous reviewers are gratefully appreciated. This research was partially supported by the National Science Foundation (NSF), USA, under grant ATM-0622745.

REFERENCES

- ARMFIELD, S. W. & PATTERSON, J. C. 1992 Wave properties of natural convection boundary layers. *J. Fluid Mech.* **239**, 195–211.
- ARMFIELD, S. W., PATTERSON, J. C. & LIN, W. 2007 Scaling investigation of the natural convection boundary layer on an evenly heated plate. *Intl J. Heat Mass Transfer* **50**, 1592–1602.
- BERGHOLZ, R. F. 1978 Instability of steady natural convection in a vertical fluid layer. *J. Fluid Mech.* **84**, 743–768.
- BOUDJEMADI, R., MAPU, V., LAURENCE, D. & LE QUERE, P. 1997 Budgets of turbulent stresses and fluxes in a vertical slot natural convection flow at Rayleigh $Ra = 10^5$ and $5.4 \cdot 10^5$. *Intl J. Heat Fluid Flow* **18**, 70–79.
- CUSHMAN-ROISIN, B. 1994 *Introduction to Geophysical Fluid Dynamics*. Prentice Hall.
- DANIELS, P. G. & PATTERSON, J. C. 1997 On the long-wave instability of natural-convection boundary layers. *J. Fluid Mech.* **335**, 57–73.
- DANIELS, P. G. & PATTERSON, J. C. 2001 On the short-wave instability of natural convection boundary layers. *Proc. R. Soc. Lond. A* **457**, 519–538.
- FEDOROVICH, E., CONZEMIUS, R., ESAU, I., KATOPODES CHOW, F., LEWELLEN, D., MOENG, C.-H., PINO, D., SULLIVAN, P. & VILÀ-GUERAU DE ARELLANO, J. 2004a Entrainment into sheared convective boundary layers as predicted by different large eddy simulation codes. In *Sixteenth Symposium on Boundary Layers and Turbulence*, (Am. Meteor. Soc., 9–13 August), Portland, Maine, CD-ROM.
- FEDOROVICH, E., CONZEMIUS, R. & MIRONOV, D. 2004b Convective entrainment into a shear-free linearly stratified atmosphere: bulk models reevaluated through large eddy simulations. *J. Atmos. Sci.* **61**, 281–295.
- FEDOROVICH, E., NIEUWSTADT F. T. M. & KAISER, R. 2001 Numerical and laboratory study of horizontally evolving convective boundary layer. Part I: Transition regimes and development of the mixed layer. *J. Atmos. Sci.* **58**, 70–86.
- GEBHART, B., JALURIA, Y., MAHAJAN, R. L. & SAMMAKIA, B. 1988, *Buoyancy-Induced Flows and Transport*. Hemisphere Publishing.
- GEORGE, W. K. & CAPP, S. P. 1979 A theory for natural convection turbulent boundary layers next to heated vertical surfaces. *Intl J. Heat Mass Transfer* **22**, 813–826.
- GILL, A. E. & DAVEY, A. 1969 Instabilities of a buoyancy-driven system. *J. Fluid Mech.* **35**, 775–798.
- LANGHAAR, H. L. 1951 *Dimensional Analysis and Theory of Models*. Robert E. Krieger Publishing Company.

- PARK, J. S. 2001 Transient buoyant flows of a stratified fluid in a vertical channel. *KSME Intl J.* **15**, 656–664.
- PARK, J. S. & HYUN, J. M. 1998 Transient behaviour of vertical buoyancy layer in a stratified fluid, *Intl J. Heat Mass Transfer* **41**, 4393–4397.
- PHILLIPS, J. R. 1996 Direct simulations of turbulent unstratified natural convection in a vertical slot for $Pr = 0.71$. *Intl J. Heat Mass Transfer* **39**, 2485–2494.
- POPE, S. B. 2000 *Turbulent Flows*. Cambridge University Press.
- SHAPIRO, A. & FEDOROVICH, E. 2004a Prandtl-number dependence of unsteady natural convection along a vertical plate in a stably stratified fluid. *Intl J. Heat Mass Transfer* **47**, 4911–4927.
- SHAPIRO, A. & FEDOROVICH, E. 2004b Unsteady convectively driven flow along a vertical plate immersed in a stably stratified fluid. *J. Fluid Mech.* **498**, 333–352.
- SHAPIRO, A. & FEDOROVICH, E. 2006 Natural convection in a stably stratified fluid along vertical plates and cylinders with temporally-periodic surface temperature variations. *J. Fluid Mech.* **546**, 295–311.
- SHCHEPETKIN, A. F. & MCWILLIAMS, J. C. 1998 Quasi-monotone advection schemes based on explicit locally adaptive dissipation. *Mon. Weather Rev.* **126**, 1541–1580.
- SMYTH, W. D. & MOUM, J. N. 2000 Length scales of turbulence in stably stratified mixing layers. *Phys. Fluids* **12**, 1327–1342.
- TENNEKES, H. & LUMLEY, J. L. 1972 *A First Course in Turbulence*. The MIT Press.
- VERSTEEGH, T. A. M. & NIEUWSTADT, F. T. M. 1998 Turbulent budgets of natural convection in an infinite, differentially heated, vertical channel. *Intl J. Heat Fluid Flow* **19**, 135–149.
- VERSTEEGH, T. A. M. & NIEUWSTADT, F. T. M. 1999 A direct numerical simulation of natural convection between two infinite vertical differentially heated walls scaling laws and wall functions. *Intl J. Heat Mass Transfer* **42**, 3673–3693.